



**HAL**  
open science

## **Complex magnetism in Ni<sub>3</sub>TeO<sub>6</sub>-type Co<sub>3</sub>TeO<sub>6</sub> and high-pressure polymorphs of Mn<sub>3-x</sub>Co<sub>x</sub>TeO<sub>6</sub> solid solutions**

Elena Solana-Madruga, Cintli Aguilar-Maldonado, Clemens Ritter, Marielle Huvé, Olivier Mentré, J. Paul Paul Attfield, Ángel M Arévalo-López

### ► To cite this version:

Elena Solana-Madruga, Cintli Aguilar-Maldonado, Clemens Ritter, Marielle Huvé, Olivier Mentré, et al.. Complex magnetism in Ni<sub>3</sub>TeO<sub>6</sub>-type Co<sub>3</sub>TeO<sub>6</sub> and high-pressure polymorphs of Mn<sub>3-x</sub>Co<sub>x</sub>TeO<sub>6</sub> solid solutions. *Chemical Communications*, 2021, 57 (20), pp.2511-2514. <10.1039/D0CC07487J>. <hal-03289757>

**HAL Id: hal-03289757**

**<https://hal.science/hal-03289757v1>**

Submitted on 18 Jul 2021

HAL is a multi-disciplinary open access archive for the deposit and dissemination of scientific research documents, whether they are published or not. The documents may come from teaching and research institutions in France or abroad, or from public or private research centers.

L'archive ouverte pluridisciplinaire HAL, est destinée au dépôt et à la diffusion de documents scientifiques de niveau recherche, publiés ou non, émanant des établissements d'enseignement et de recherche français ou étrangers, des laboratoires publics ou privés.



HAL Authorization

## Complex magnetism in Ni<sub>3</sub>TeO<sub>6</sub>-type Co<sub>3</sub>TeO<sub>6</sub> and high-pressure polymorphs of Mn<sub>3-x</sub>Co<sub>x</sub>TeO<sub>6</sub> solid solutions.

Received 00th January 20xx,  
Accepted 00th January 20xx

Elena Solana-Madruga,<sup>a,b,\*</sup> Cintli Aguilar-Maldonado,<sup>a</sup> Clemens Ritter,<sup>c</sup> Marielle Huvé<sup>a</sup>, Olivier Mentré<sup>a</sup> J. Paul Attfield<sup>b</sup> and Ángel M. Arévalo-López<sup>a\*</sup>.

DOI: 10.1039/x0xx00000x

[www.rsc.org/](http://www.rsc.org/)

**New Ni<sub>3</sub>TeO<sub>6</sub>-type (NTO) and double perovskite (DPv) polymorphs of Co<sub>3</sub>TeO<sub>6</sub> are synthesised at pressures of 15 GPa. A complex elliptic helical magnetic order is observed in the NTO polymorph (T<sub>N1</sub> = 58 K) that reorientates (42 K) and further splits (T<sub>N2</sub> = 23.5 K) creating a coexisting helix. Increasing Co content within the Mn<sub>3-x</sub>Co<sub>x</sub>TeO<sub>6</sub> system changes the dominant DPv phase to NTO structural type and drastically modifies the magnetic behaviour. DPv Co<sub>3</sub>TeO<sub>6</sub> is the first A-site double cobaltite.**

High-pressure and high-temperature synthesis has proven to be of wide interest in the search for new materials with notable properties such as multiferrocity. A-site ABO<sub>3</sub> and related manganites are able to crystallise in perovskite and corundum related structures with varied magnetic and electrical properties. For instance, localized d<sup>5</sup> (Mn<sup>2+</sup>) and itinerant d<sup>1</sup> electrons (V<sup>4+</sup>) coexist in MnVO<sub>3</sub>.<sup>1</sup> High pressure Mn<sub>2</sub>BB'O<sub>6</sub> double perovskites (DPvs) show a plethora of magnetic behaviours, with simple antiferromagnetic (AFM),<sup>2-5</sup> collinear,<sup>6</sup> perpendicular<sup>7</sup> and continuously rotating ferrimagnetic structures<sup>8</sup> and more complex incommensurate-elliptical helices.<sup>9</sup>

The stacking of honeycomb / triangular magnetic sublattices in ordered-corundum structures such as Ni<sub>3</sub>TeO<sub>6</sub>-type (NTO), induces a strong magnetic frustration, usually resulting in the formation of incommensurate helical magnetic structures,<sup>10</sup> sometimes with thermal dependence and lock-in of their propagation vector<sup>2</sup> at low temperatures.<sup>11</sup>

Ambient pressure M<sub>3</sub>TeO<sub>6</sub> (M = Mn and Co) phases crystallise in distorted corundum-based structures, also showing complex magnetic behaviours. Mn<sub>3</sub>TeO<sub>6</sub>-I (*R*-3) shows an elliptical helix and a sinusoidal spin density wave

coexisting below 24 K.<sup>12</sup> It also shows multiferroic properties below 21 K.<sup>13</sup> Co<sub>3</sub>TeO<sub>6</sub>-I (*C2/c*) has 5 independent Co sites, providing a rich magnetic phase diagram<sup>14,15</sup> with subsequent magnetic transitions originating an incommensurate [0 k<sub>y</sub> k<sub>z</sub>], a [0 0 0] (k<sub>0</sub> from here) and a sinusoidal [0 ½ ¼] magnetic structures.<sup>16</sup> It is also notable for showing a magnetic field-induced electrical polarisation.<sup>17,18</sup>

The high-pressure DPv modification of Mn<sub>3</sub>TeO<sub>6</sub> (Mn<sub>2</sub>MnTeO<sub>6</sub>-II, *P2<sub>1</sub>/n*), was recently reported as a collinear AFM with k = [½ 0 ½] below 36 K with an unusually large frustration index of 5.1 due to the rock-salt order of the d<sup>5</sup> Mn<sup>2+</sup> cations with the diamagnetic d<sup>10</sup> Te<sup>6+</sup>.<sup>3</sup> In this communication, we report the high-pressure phase modification of Co<sub>3</sub>TeO<sub>6</sub> (HP-Co<sub>3</sub>TeO<sub>6</sub>) and its combination with DPv-Mn<sub>3</sub>TeO<sub>6</sub> into the HP-Mn<sub>3-x</sub>Co<sub>x</sub>TeO<sub>6</sub> series. Co<sub>3</sub>TeO<sub>6</sub> presents both NTO- and DPv-type structures from high pressure-high temperature synthesis, with predominance of NTO at the applied 15 GPa synthesis pressure and evidence of higher stability of the denser DPv polymorph as a function of pressure. The NTO polymorph shows an incommensurate elliptical helix below 58 K. The magnetic propagation vector shifts with temperature and locks at 23 K, where it splits creating a coexisting circular helix. Dealing with the mixed Mn/Co compounds, the NTO-type structure is retained for Co-rich members but changes to DPv polymorph at the Mn-rich side of the system. The presence of small proportions of either Mn<sup>2+</sup> (d<sup>5</sup>, S = 5/2) or Co<sup>2+</sup> (d<sup>7</sup>, S = 3/2) cations induces dramatic magnetic changes, reflecting the essential role of t<sub>2g</sub> orbitals in the set of magnetic exchanges.

HP-Mn<sub>3-x</sub>Co<sub>x</sub>TeO<sub>6</sub> samples were prepared for x = 0.5, 1, 1.5, 2, 2.5 and 3 by high-pressure high-temperature phase transformation at 8, 10, 10, 12, 13 and 15 GPa respectively as detailed in ESI. Note that higher pressures are needed to stabilise larger amounts of smaller Co<sup>2+</sup> in the same polymorph (0.90 and 0.745 Å vs. 0.96 and 0.83 Å for Mn<sup>2+</sup> in 8- and 6- fold coordination).<sup>19</sup>

The NTO-type Co<sub>3</sub>TeO<sub>6</sub> structure has been refined from 300 K high-resolution NPD data (λ = 1.54 Å) collected at D20 at ILL. Rietveld fit results reveal a fully ordered NTO-type

<sup>a</sup> Univ. Lille, CNRS, Centrale Lille, ENSCL, Univ. Artois, UMR 8181 - UCCS - Unité de Catalyse et Chimie du Solide, F-59000 Lille, France. \* [elena.solanamadruga@univ-lille.fr](mailto:elena.solanamadruga@univ-lille.fr) and [angel.arevalo-lopez@univ-lille.fr](mailto:angel.arevalo-lopez@univ-lille.fr)

<sup>b</sup> Centre for Science at Extreme Conditions (CSEC) and School of Chemistry, The University of Edinburgh. EH9 3FD, U.K.

<sup>c</sup> Institut Laue-Langevin, Avenue des Martyrs 71, 32042, Grenoble Cedex, France.

‡ Electronic Supplementary Information (ESI) available: supporting figures and tables. See DOI: 10.1039/x0xx00000x

structure with four independent cation sites (S.G.  $R\bar{3}$ ); see Figure 1a and Table 1. It consists of alternated  $ab$  honeycomb layers of  $\text{Co}_1\text{O}_6/\text{TeO}_6$  ( $\text{Co}_2\text{O}_6/\text{Co}_3\text{O}_6$ ) edge sharing octahedra.

Together, it forms  $\text{Co}_1\text{O}_6/\text{Co}_2\text{O}_6$  ( $\text{Co}_3\text{O}_6/\text{TeO}_6$ ) face sharing dimers along  $c$  and  $\text{Co}_1\text{O}_6/\text{Co}_3\text{O}_6$  corner sharing along the  $[012]$  direction. Octahedral distortions, calculated from  $\Delta = (1/6) \sum [(d_i - d_{\text{av}})/d_{\text{av}}]^2$ , reveal the highest distortion for  $\text{Co}_3\text{O}_6$  ( $7.17 \times 10^{-3}$ ) due to its Coulomb repulsions against the faced non-polarisable  $d^{10} \text{Te}^{6+}$  cation. Such distortion is cushioned in the  $\text{Co}_1$ - $\text{Co}_2$  dimer. Bond Valence Sum calculations confirm the  $2+$  and  $6+$  oxidation states for  $\text{Co}$  and  $\text{Te}$  in all sites, and thus the nominal  $\text{Co}^{2+}_3\text{Te}^{6+}\text{O}_6$  stoichiometry. The presence of a possible superstructure or any short-range order for  $\text{NTO-Co}_3\text{TeO}_6$  was checked and ruled out by means of transmission electron microscopy (ESI). Evidence of an even higher-pressure  $\text{Co}_3\text{TeO}_6$  polymorph with DPv structure similar to that of  $\text{Mn}_3\text{TeO}_6$ -II was observed and considered in the refinement and discussed below. The existence of both NTO and DPv phases throughout the HP- $\text{Mn}_{3-x}\text{Co}_x\text{TeO}_6$  series suggest the possibility to quench both phases under different synthesis conditions. However,  $\text{DPv} \rightarrow \text{NTO}$  phase transition at decompression may be possible, as observed in  $\text{ScFeO}_3$ ,<sup>20</sup> and cannot be discarded. In-situ HP diffraction studies would clarify this matter.

Figure 1b shows the bulk magnetic behaviour of HP- $\text{Co}_3\text{TeO}_6$ . The Curie-Weiss fit to the inverse susceptibility results in  $\theta = -73 \text{ K}$  and  $\mu_{\text{eff}} = 5.3 \mu_{\text{B}} / \text{Co}^{2+}$ , showing a large contribution of spin orbit coupling (SOC) and predominant AFM interactions. FC-ZFC susceptibility curves show a first transition at  $T_{\text{N}1} = 58 \text{ K}$ , a maximum at  $42 \text{ K}$  (increase of the reorientation as discussed below) and a second transition at  $T_{\text{N}2} = 23.5 \text{ K}$ . Hysteresis loops in the inset of Fig. 1b confirm the presence of a ferromagnetic component of  $\sim 1 \mu_{\text{B}}$  at  $35 \text{ K}$  with hysteretic behaviour at  $2 \text{ K}$ . The presence of minor

Table 1. Atomic positions and main interatomic distances and angles from the Rietveld fit of  $\text{NTO-Co}_3\text{TeO}_6$  against 300 K NPD data. S.G.  $R\bar{3}$ ,  $a = 5.1874(2) \text{ \AA}$ ,  $c = 13.8015(7) \text{ \AA}$ .

Site	x	Y	z	$B_{\text{iso}}(\text{\AA}^2)$	Occ
Co1 (3a)	0.0	0.0	0.062 <sup>a</sup>	0.21(7)	1.0
Co2 (3a)	0.0	0.0	0.264(2)	0.21*	1.0
Co3 (3a)	0.0	0.0	0.540(3)	0.21*	1.0
Te (3a)	0.0	0.0	0.765(2)	0.21*	1.0
O1 (9b)	0.337(1)	0.040(1)	0.169(2)	0.9(2)	1.0
O2 (9b)	0.329(1)	0.367(1)	0.337(2)	0.1(1)	1.0
$3x d_{\text{Co}1\text{-O}1}(\text{\AA})$	2.21(2)		$3x d_{\text{Co}3\text{-O}1}(\text{\AA})$	2.00(1)	
$3x d_{\text{Co}1\text{-O}2}(\text{\AA})$	2.02(1)		$3x d_{\text{Co}3\text{-O}2}(\text{\AA})$	2.37(5)	
$3x d_{\text{Co}2\text{-O}1}(\text{\AA})$	2.11(3)		$3x d_{\text{Te-O}1}(\text{\AA})$	1.89(3)	
$3x d_{\text{Co}2\text{-O}2}(\text{\AA})$	2.07(3)		$3x d_{\text{Te-O}2}(\text{\AA})$	2.02(4)	
$\Delta\text{Co}1 \times 10^3$	2.02 <sup>b</sup>		$\Delta\text{Co}3 \times 10^3$	7.17 <sup>b</sup>	
$\Delta\text{Co}2 \times 10^3$	0.09 <sup>b</sup>		$\Delta\text{Te} \times 10^3$	1.11 <sup>b</sup>	
$\text{BVS}_{\text{Co}1}$	1.98		$\text{BVS}_{\text{Co}3}$	1.80	
$\text{BVS}_{\text{Co}2}$	2.04		$\text{BVS}_{\text{Te}}$	5.45	

<sup>a</sup> Co1 site is used as the refence for the cell. <sup>b</sup>  $\Delta$  values calculated from  $(1/6) \sum [(d_i - d_{\text{av}})/d_{\text{av}}]^2$ . \* Constrained to Co1.

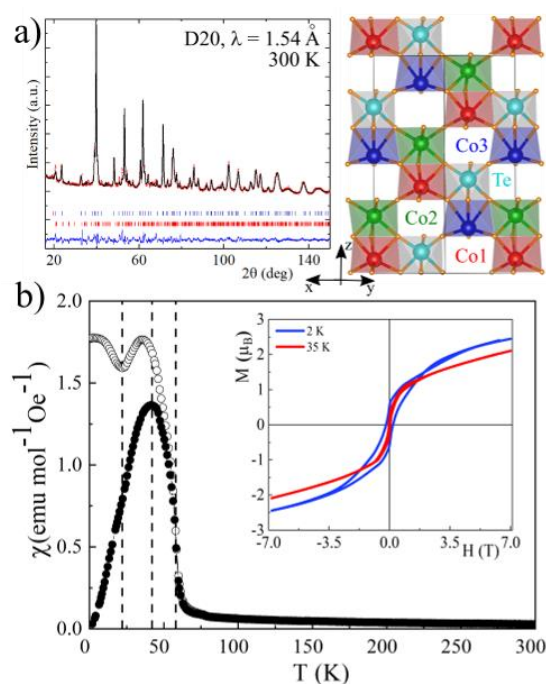


Fig. 1. a) Rietveld fit of the 300 K NPD data for HP- $\text{Co}_3\text{TeO}_6$ . First and second row of Bragg tick marks refer to 85.5% of NTO- and 14.5 % of DPv-polymorphs (see text). NTO-type structure shown on the right panel. b) FC-ZFC magnetic susceptibility curves, shown as open and closed circles respectively. Vertical broken lines mark transitions observed in the NPD data. Inset shows magnetisation-field loops.

(14.5%) AFM DPv HP phase with lower  $T_{\text{N}}$  is masked by the bulk (ferri)magnetic behaviour of the main NTO phase. The unambiguous identification of both polymorphs from SXR and NPD along with the stability of the refinements against all NPD data sets and difference patterns confirms the feasibility of the magnetic models discussed below.

Low temperature NPD data for HP- $\text{Co}_3\text{TeO}_6$  sample are shown in Figure 2. The magnetic peaks at  $40 \text{ K}$  can be indexed with coexisting propagation vectors  $k_{z1} = [0 \ 0 \ 0.2213(6)]$  and  $k_0 = [0 \ 0 \ 0]$ . The presence of the main (003) magnetic and satellite peaks indicates that spins are mainly perpendicular to the  $c$  axis for both  $k$  vectors. Their combination could signify coexistence of a collinear and a helical magnetic structure. However, the simultaneous appearance of both sets of magnetic peaks for all NTO-type HP- $\text{Mn}_{3-x}\text{Co}_x\text{TeO}_6$  compounds suggests a single magnetic phase. The combination of collinear and helical spin structures modulates the magnetic moments in the  $ab$  plane, giving rise to an elliptical helix.

The evolution of  $k_{z1}$  upon cooling shows its splitting at  $T_{\text{N}2}$  into  $k_{z1}$  and  $k_{z2}$ , both vectors freezing at  $16 \text{ K}$  with refined values of  $k_{z1} = 0.3988(9)$  and  $k_{z2} = 0.4742(8)$  at  $1.5 \text{ K}$ , see Figure 2.

The magnetic structures were refined against NPD difference patterns  $40 \text{ K} - 80 \text{ K}$  ( $k_{z1}+k_0$ ) and  $1.5 \text{ K} - 80 \text{ K}$  ( $k_{z1}+k_0$ ,  $k_{z2}$ ), see ESI for details. The elliptical helix at  $40 \text{ K}$  ( $R_{\text{mag}} = 8.70 \%$ ) presents modulated magnetic moments

within the *ab* plane varying between 0.48(1) and 2.44(1)  $\mu_B$ . One magnetic layer is projected along [001] in Fig. 3a (top). The fit of the 1.5 K – 80 K difference pattern reveals the contribution of the  $k_0$  vector only to  $k_{z1}$  phase, while the new  $k_{z2}$  phase has pure helical topology. The magnetic moments in each of the helical phases (following each incommensurate  $k$  vector) were constrained to the same values for stability of the refinements. The lowest temperature fit results in maximum values of 2.87(1)  $\mu_B$ , the modulated moment of the elliptical phase increasing from 0.98(1)  $\mu_B$ . The phase proportion from this fit refines to 56 % elliptical and 44 % circular helices, with magnetic reliability factors  $R_{\text{mag}} = 2.18\%$  and  $3.28\%$  respectively.

Figure 2b (top) shows the thermal evolution of the maximum magnetic moment in the elliptical phase, equal to the total magnetic moment in the circular helix. The fit to the critical law  $\mu(T) = \mu(0) * [1 - (T/T_{N1})]^\beta$  in the  $(T_{N1}/2) < T < T_{N1}$  temperature range results in  $T_{N1} = 58.7(3)$  K,  $\mu(0) = 3.04(9)$   $\mu_B$ , in good agreement with the expected value for  $S = 3/2$  high spin  $\text{Co}^{2+}$  cations, and  $\beta = 0.22(2)$ , confirming the magnetic 2D-XY behaviour. The DPV- $\text{Co}_3\text{TeO}_6$  minor phase was included in the magnetic refinements using  $k = [\frac{1}{2} 0 \frac{1}{2}]$  similar to that of  $\text{Mn}_3\text{TeO}_6\text{-II}$ . Further studies will be addressed to the full magnetic characterisation of this DPV polymorph as a pure phase.

The spin angles between Co1-Co2/Co2-Co3 sites at 1.5 K are  $-133(1)^\circ/179(1)^\circ$  and  $-172(1)^\circ/154(1)^\circ$  for the elliptical and circular helices respectively. The nearly ideal  $180^\circ$  AFM and the  $\sim 120^\circ$  angle, often stabilised in frustrated trigonal compounds, reflects the strong competition of the involved interactions (see below) and justifies the low temperature separation into two coexisting magnetic phases. Other possible driving forces could be local strains or minor chemical disorder effects (e.g. local Co/Te antisites) too small to be detected. At least dealing with a phase segregation at

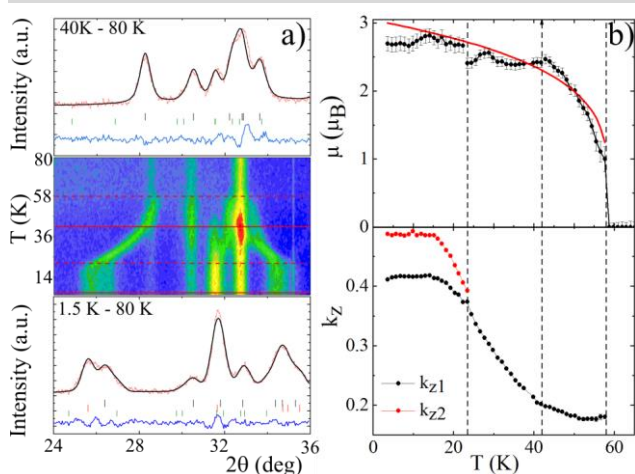


Figure 2. a) Rietveld fits of the HP- $\text{Co}_3\text{TeO}_6$  NPD 40 K – 80 K (top) and 1.5 K – 80 K (bottom) difference patterns. Middle panel shows the 2D thermodiffraction, with dashed red lines at  $T_{N1}$  and  $T_{N2}$  and solid lines for fitted  $T$ . b) Thermal evolution of the magnetic moment and  $k_z$  vector. Fit to the critical law for the magnetic moments is shown as a red line.

the microscopic scale, a sensitive decrease of magnetic correlation lengths is expected across  $T_{N2}$ . Such correlation change was checked by the broadening of magnetic satellites in  $\Delta L \sim 150$  nm, as calculated using the Scherrer formula.

The remarkable magnetic complexity of NTO- $\text{Co}_3\text{TeO}_6$ , unambiguously intrinsic to the NTO phase according to the stability of all Rietveld fits against our NPD data, has motivated the study of the HP- $\text{Mn}_{3-x}\text{Co}_x\text{TeO}_6$  system. The series shows a coherent evolution, crystallising with the DPV structure for  $x < 1.5$  and with NTO structure for  $x > 1.5$  (ESI). The  $x = 1.5$  intermediate composition shows phase coexistence refined to 88.4 % DPV vs. 11.6 % NTO from NPD data collected under high resolution at 300 K. The use of 12–13 GPa could solely drive to the rhombohedral polymorph, while for  $x = 3$  small amounts of DPV (14.5%) are observed when prepared at 15 GPa. This suggests the accessibility to the DPV polymorph for the complete series at higher pressures. DPV- $\text{Co}_3\text{TeO}_6$  is remarkable as the first A-site double cobaltite, and further studies will be required to isolate it for a complete characterisation.

The atomic positions, summarised in ESI tables, show full cation order among 2+/6+ B-site cations and site preference for the larger  $\text{Mn}^{2+}$  at the A sites. Among the NTO phases, cation order/site preference is also observed. The magnetic behaviour of the solid solution shows a coherent evolution in transition temperature and refined magnetic moments at 1.5 K, as summarised in Table 2 and the magnetic phase diagram in Figure 3b. Among the DPV polymorphs, two AFM structures with  $k = [\frac{1}{2} 0 \frac{1}{2}]$  (like that of  $\text{Mn}_3\text{TeO}_6\text{-II}$ )<sup>3</sup> and  $k_0$  (Fig. 3c) are observed, both with collinear spins in the *ac* plane. All the NTO phases show coexistence of  $k_0$  and an incommensurate  $k_z$  propagation vectors with simultaneous orders, revealing elliptical helix magnetic structures like that of NTO- $\text{Co}_3\text{TeO}_6$ . Surprisingly, no thermal dependence of  $k_z$  was observed for mixed Mn/Co phases (ESI).

Table 2. Magnetic transition temperatures, propagation vectors, effective magnetic moment per  $\text{M}^{2+}$  ( $\mu_{\text{eff}}$ ) from Curie-Weiss fits and refined magnetic moments in A and B sites ( $\mu_{A/B}$ ) for HP- $\text{Mn}_{3-x}\text{Co}_x\text{TeO}_6$  system at 1.5 K. The refined magnetic moments for the NTO phases show the total/maximum value for the  $k_z$  phase.

x	$T_N$ (K)	$k$	DPV/NTO (%)	$\mu_{\text{eff}}$ ( $\mu_B$ )	$\mu_{A/B}$ ( $\mu_B$ )
0	36	$[\frac{1}{2} 0 \frac{1}{2}]$	100	5.6	4.8(6)/3.9(1)
0.5	31	$[\frac{1}{2} 0 \frac{1}{2}]$	100	x	3.61(2)/2.42(2)
	23	$[0 0 0]$			3.58(1)/2.40(2)
1.0	27	$[0 0 0]$	100	5.4	3.21(1)/1.84(2)
1.5	25	$[0 0 0]$	88.4(1)	5.9	3.48(1)/1.25(3)
	67	$k_0 + k_z = 0.080(1)$	11.6(1)		3.89(4)
2.0	72	$k_0 + k_z = 0.094(1)$	100	5.3	4.47(1)
2.5	66	$k_0 + k_z = 0.117(1)$	100	5.7	4.13(1)
3.0	47	$[\frac{1}{2} 0 \frac{1}{2}]$	14.5(1)	5.3	2.87(1)
	58	$k_0 + *k_{z1} = 0.3988(9)$	85.5(1)		
	23	$*k_{z2} = 0.4742(8)$			

Expected  $\mu_{\text{eff}} = 5.92 \mu_B/\text{Mn}^{2+}$  / up to  $6.63 \mu_B/\text{Co}^{2+}$  considering SOC. \* Experimental issues prevent CW fit. \* T-dependent.

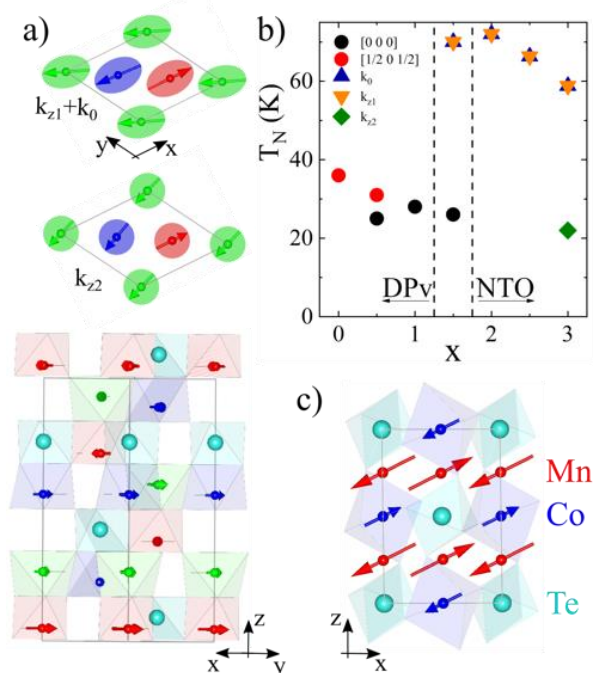


Figure 3. a) [001] projection of the elliptical (top) and circular (middle) magnetic structures of NTO-Co<sub>3</sub>TeO<sub>6</sub> at 1.5 K. The bottom panel shows half-cell of the longer  $k_{z2}$  phase along [110]. b) Phase diagram for the HP-Mn<sub>3-x</sub>Co<sub>x</sub>TeO<sub>6</sub> solid solution c)  $k_0$  magnetic structure of the DPV-Mn<sub>2</sub>CoTeO<sub>6</sub>.

The cation order and the progressive evolution from  $d^5$  to  $d^7$  weakens the superexchange interactions through oxygen in both polymorphs and more importantly the direct interactions via  $t_{2g}$ - $t_{2g}$  orbital overlap in face sharing Co1-Co2 and edge sharing Co2-Co3 sites in the NTO phases. This induces the strongest magnetic frustration for larger Co content, justifying the decreasing  $T_N$  and the simple thermal evolution of  $1.5 < x < 3$  compounds.

In conclusion, a new high pressure Co<sub>3</sub>TeO<sub>6</sub> R3 NTO polymorph has been prepared. Its complex magnetic behaviour is dominated by the strong frustration of the stacked honeycomb and triangular magnetic sublattices. Below 58 K an elliptical helix magnetic structure with temperature dependent  $k_{z1}$  vector rotates and splits below 23 K, where it coexists with a  $k_{z2}$  circular helix. Evidence for a higher pressure DPV-Co<sub>3</sub>TeO<sub>6</sub> with  $k = [\frac{1}{2}\ 0\ \frac{1}{2}]$ , notable as the first A-site double cobaltite, will be further studied. The HP-Mn<sub>3-x</sub>Co<sub>x</sub>TeO<sub>6</sub> system between NTO-Co<sub>3</sub>TeO<sub>6</sub> and Mn<sub>3</sub>TeO<sub>6</sub>-II has a coherent structural and magnetic evolution from AFM DPV ( $x < 1.5$ ) to elliptical NTO ( $x > 1.5$ ). The presence of any Mn<sup>2+</sup> ( $d^5$ ,  $S = 5/2$ ) in the NTO polymorphs prevents the thermal dependence of their incommensurate  $k_z$  vector and the presence of any Co<sup>2+</sup> ( $d^7$ ,  $S = 3/2$ ) in the DPV phases changes the  $k = [\frac{1}{2}\ 0\ \frac{1}{2}]$  AFM structure into a different  $k_0$  one. These dramatic magnetic effects reflect the essential role of  $t_{2g}$  orbitals in the magnetic behaviour of these compounds. Recently, Co<sub>3</sub>TeO<sub>6</sub> has also been prepared at 5 GPa and their findings agree with our results.<sup>21</sup> However, those authors did not observe nor predict the DPV Co<sub>3</sub>TeO<sub>6</sub> higher pressure phase.

We thank EPSRC for support, and Diamond and the ILL for beamtime. Stephen Thompson is acknowledged for assistance on I11 data collection. AMAL thanks the ANR-AMANTS project (19-CE08-0002-01). CAM thanks CONACyT-Mexico for a post-doctoral fellowship (CVU 350841). Chevreul Institute (FR 2638), Region Hauts-de-France, and FEDER for funding the X-ray diffractometers, electron microscope and the PPMS magnetometer.

### Conflicts of interest

There are no conflicts of interest to declare.

### Notes and references

- M. Markkula, A. M. Arévalo-López, A. Kusmartseva, J.A. Rodgers, C. Ritter, H. Wu, J.P. Attfield, *Phys. Rev. B*, 2011, **84**, 094450.
- A. J. Dos santos-García, E. Solana-Madruga, C. Ritter, D. Ávila-Brande, O. Fabelo, R. Sáez-Puche, *Dalton Trans.*, 2015, **44**, 10665.
- A.M. Arévalo-López, E. Solana-Madruga, C. Aguilar-Maldonado, C. Ritter, O. Mentré, J.P. Attfield, *Chem. Commun.* 2019, **55**, 14470-14473.
- C. E. Frank, E. E. McCabe, F. Orlandi, P. Manuel, X. Tan, Z. Deng, M. Croft, V. Cascos, T. Emge, H. L. Feng, S. Lapidus, C. Jin, M. X. Wu, M. R. Li, S. Ehrlich, S. Khalid, N. Quackenbush, S. Yu, D. Walker, M. Greenblatt, *Chem. Commun.* 2019, **55**, 3331-3334.
- E. Solana-Madruga, A.J. Dos santos-García, A.M. Arévalo-López, D. Ávila-Brande, C. Ritter, J.P. Attfield, R. Sáez-Puche, *Dalton Trans.*, 2015, **44**, 20441-20448.
- A.M. Arévalo-López, G.M. McNally, J.P. Attfield, *Angew. Chem. Int. Ed.* 2015, **54**, 12074.
- A. M. Arévalo-López, F. Stegemann, J. P. Attfield, *Chem. Commun.*, 2016, **52**, 5558.
- E. Solana-Madruga, K. N. Alharbi, M. Herz, P. Manuel, J. P. Attfield, *Chem. Commun.*, 2020, **56**, 12574-12577.
- A. J. Dos santos-García, C. Ritter, E. Solana-Madruga, R. Sáez-Puche, *J. Phys.: Condens. Matter*, 2013, **25**, 206004.
- A. J. Dos santos-García, E. Solana-Madruga, C. Ritter, A. Andrada-Chacón, J. Sánchez-Benítez, F. J. Mompean, M. Garcia-Hernandez, R. Sáez-Puche, R. Schmidt, *Angew. Chem. Int. Ed.* 2017, **56**, 4438-4442.
- Á. M. Arévalo-López, E. Solana-Madruga, E. P. Arévalo-López, D. Khalyavin, M. Kepa, A. J. Dos santos-García, R. Sáez-Puche, J. P. Attfield, *Phys. Rev. B*, 2018, **98**, 214403.
- L. Zhao, Z. Hu, C.-Y. Kuo, T.-W. Pi, M.-K. Wu, L.H. Tjeng, A.C. Komarek, *Phys. Status Solidi RRL* 2015, **9**, 730.
- S.A. Ivanov, C. Ritter, P. Nordblad, R. Tellgren, M. Weil, V. Carolus, T. Lottermoser, M. Fiebig, R. Mathieu, *J. Phys. D: Appl. Phys.* 2017, **50**, 085001.
- J.L. Her, C.C. Chou, Y.H. Matsuda, K. Kindo, H. Berger, K.F. Tseng, C.W. Wang, H.D. Yang, *Phys. Rev. B*, 2011, **84**, 235123.
- C.-W. Wang, C.-H. Lee, C.-Y. Li, C.-M. Wu, W.-H. Li, C.-C. Chou, H.-D. Yang, J.W. Lynn, Q. Huang, A.B. Harris, H. Berger, *Phys. Rev. B*, 2013, **88**, 184427.
- S. A. Ivanov, R. Tellgren, C. Ritter, P. Nordblad, R. Mathieu, G. André, E.D. Politova, M. Weil, *Mat. Res. Bull.* 2012, **47**, 63.
- M. Hudl, R. Mathieu, S.A. Ivanov, M. Weil, V. Carolus, T. Lottermoser, M. Fiebig, Y. Tokunaga, Y. Taguchi, Y. Tokura, P. Nordblad, *Phys. Rev. B*, 2011, **84**, 180404(R).
- A.B. Harris, *Phys. Rev. B*, 2012, **85**, 100403(R).
- R. D. Shannon, C. T. Prewitt, *Acta Cryst. B*, 1969, **25**, 925.
- T. Kawamoto, K. Fujita, I. Yamada, T. Matoba, S. J. Kim, P. Gao, X. Pan, S. D. Findlay, C. Tassel, H. Kageyama, J. Hester, T. Irifune, H. Akamatsu, K. Tanaka, *J. Am. Chem. Soc.* 2014, **136**, 15291.
- Y. Han, M. Wu, C. Gui, C. Zhu, Z. Sun, M.-H. Zhao, A. A. Savina, A. M. Abakumov, B. Wang, L. H. He, J. Chen, M. Croft, S. Ehrlich, S. Khalid, Z. Deng, C. Jin, C. P. Grams, J. Hemberger, X. Wang, J. Hong, U. Adem, M. Ye, S. Dong, M.-R. Li, *npj Quantum Materials* 2020, **5**, 92.